



PONTIFICIA UNIVERSIDAD CATÓLICA DE CHILE

FACULTAD DE FÍSICA

INSTITUTO DE ASTROFÍSICA

TESTING MODIFIED GRAVITY USING A MARKED CORRELATION FUNCTION

POR

JOAQUÍN ARMIJO TORRES

PROFESOR GUÍA : Dr. Nelson Padilla

: Dr. Yan-Chuan Cai

PROFESOR CORRECTOR : Dr. Felipe Barrientos

Dr. Rolando Dünner

June, 2018

SANTIAGO, CHILE

©2018, JOAQUÍN ARMIJO TORRES

Se autoriza la reproducción total o parcial, con fines académicos , por cualquier medio o procedimiento, incluyendo la cita bibliográfica del documento.

*Dedicado a todos los que intentan,
intentan hasta que lo logran.*

Acknowledgement

I decided to write this acknowledgements full in English this time. My master degree was a short but difficult step in my life, and it happens so fast that I did not take time to think about it. I want to thank to all the people that made this 2 years more easy for me.

First, my advisors, Nelson and Cai for all the constant support provided during this work, and also thanks to the committee, for taking some time to read and check this thesis. Special thanks to Enrique, for helping me to prepare some explicative plots that I did include in my presentation.

Secondly, thanks to my family and friends, they are too many to mention each of you in these paragraphs, but you know who you are. All my love to my Ema, who gave me her unconditional love and care that I needed all this time.

It was a hard road to follow, with so much sacrifice and difficulties, but a harder one is coming. I am pretty sure that all the experience I did gather on this time, will serve on purpose to build a brighter path to find the brightest future. For all this, my acknowledgement to all the people who join me on this road.

Contents

1	Introduction	1
2	Theory and simulations	4
2.1	The $f(R)$ model of gravity	4
2.2	Simulations and mock galaxy catalogues	9
3	The Marked Correlation Function	12
3.1	Marked pairs computation	12
3.2	A mark based on local density	14
3.3	A mark based on halo mass	18
4	Conclusions and Discussion	22
4.1	Discussion	22
4.2	Conclusions	24
4.3	Proposed application to data	26

List of Figures

2.1	Dark matter particle simulations in a box with size of 64 Mpc/ h , from Zhao, Li & Koyama (2011). A comparison between Λ CDM universe and modified gravity. Bottom panel are the two $f(R)$ models used in this work, with $ f_{R0} = 10^5, 10^6$ respectively.	6
2.2	The two-point correlation function ξ of the different model in the simulations. The shaded region indicates the 1σ confidence of GR model. As reported in Cautun et al. (2018) the clustering deviations between MG and GR models are below the 5%.	8
2.3	The mean number of galaxies, $\langle N \rangle$, as a function of halo mass, M for F5, F6 and GR models. The secondary panel shows the ratio of the $f(R)$ models HOD to the GR one. This parameters are used to match the clustering and number density of galaxies as is mentioned on Cautun et al. (2018)	10
3.1	The distribution of the host halo mass M sampled by the HOD galaxies for different models as labelled in the legend. The dashed line indicates mean value for GR.	13
3.2	Distribution of galaxy local densities estimated using a Voronoi tessellation method. Only the range of below the mean density is shown for better illustration.	16

3.3	The marked correlation function $\mathcal{M}(r)$ using the local density ρ as the mark. This plot shows the examples for $\mathcal{M} = \rho^p$, with $p = \pm 0.5$ in solid (-0.5) and dashed lines (0.5). The lower panel shows the ratios of marked correlation functions between $f(R)$ and GR. The shaded regions correspond to the errors on the mean corresponding to a volume of $\sim 1(h^{-1}\text{Gpc})^3$ estimated using the Jackknife method. The dark and light shaded regions are for the case of $p = -0.5$ and $p = 0.5$ respectively. . . .	17
3.4	Similar to Fig. 3.3 but showing the marked correlation function using the host halo mass of galaxies M as the mark, $m = M^p$. The solid and dashed curves shows the case for $p = 0.1$ and $p = -0.1$ respectively. The dark and light shaded regions show the 1σ errors for these two cases. The panels show the different cases: using the host halo mass as mark adding 0.1 dex uncertainty to the masses (A), adding 0.2 dex uncertainty (B), using only 8 mass bins to generate the marks and 0.1 dex uncertainty (C) and adding 0.2 dex uncertainty (D).	21
4.1	Different χ_ν^2 as function of the free parameter p for the mass-marked correlation function in F5 (<i>left</i>) and F6 (<i>right</i>). The 5 boxes show a wide range of possible χ_ν^2 values in a range of $p = [-10, 10]$	23
4.2	The marked-cross-correlation function between GC centers and galaxies for different models. A combination of marks is explored in this case, using $m_{GC} = M^p$ and $m_g = \rho^p$. The shaded region is the GR errorbars estimations showing the 1σ confidence estimation.	28

Resumen

En teorías de gravedad modificada que presentan mecanismo de apantallamiento camaleón, la fuerza de la quinta fuerza depende del ambiente donde es gatillada. Esto induce una dependencia del entorno en la formación de la estructura a gran escala, que difiere del Universo Λ CDM. Se muestra que tales diferencias pueden ser capturadas por medio de una función de correlación marcada. Con la función de correlación de galaxias y su número de densidad calibrado para ser el mismo entre los modelos $f(R)$ y Λ CDM, en simulaciones numéricas, mostramos que la función de correlación marcada usando la densidad local o la masa de los halos para marcar las galaxias, contiene información extra y puede ser usada para probar estas teorías. Discutimos las posibles aplicaciones de este estudio estadístico in observaciones. Esta tesis reproduce texto de Armijo et al. (2018) literalmente.

Abstract

In theories of modified gravity with the chameleon screening mechanism, the strength of the fifth force depends on the environment. This induces an environment dependence of structure formation, which differs from Λ CDM. We show that these differences can be captured by the marked correlation function. With the galaxy correlation functions and number densities calibrated to match between $f(R)$ and Λ CDM models in simulations, we show that the marked correlation functions from using either the local density or the halo mass to mark galaxies extra information is encoded, and can be used to test these theories. We discuss possible applications of these statistics in observations. This thesis reproduces text from Armijo et al. (2018) verbatim.

Chapter 1

Introduction

The current cosmological paradigm establishes that the Universe is expanding due to the influence of the mysterious component named dark energy, which arises in General Relativity (GR), as a cosmological constant Λ . Theories of modified gravity (MG) were proposed as alternatives to the Λ -cold-dark-matter (Λ CDM) paradigm to explain the late-time cosmic acceleration without using Λ , but with external degrees of freedom that produce a similar effect on the Universe. Such models work as an extension to the standard GR model and they can be used to study the effects of gravity at large-scales.

In light of the recent detection of gravitational waves from the binary neutron star merger GW170817 and simultaneous measurement of its optical counterpart GRB170817A, several popular classes of MG models are ruled out (e.g. Lombriser & Taylor, 2016; Baker et al., 2017; Sakstein & Jain, 2017; Ezquiaga & Zumalacarregui, 2017; Creminelli & Vernizzi, 2017). These kind of models modified the propagation velocity of gravitational waves in the vacuum, which is not consistent with the current measurements (Abbott et al., 2017). Nevertheless, many other models remain viable and would affect the growth of large-scale structure, such as Brans-Dicke type theories, including derivative-coupling theories such the normal-branch Dvali-Gabadadze-Porrati (nDGP) model (Dvali, Gabadadze & Porrati, 2000), Chameleon models, including $f(R)$ grav-

ity (De Felice & Tsujikawa, 2010), and more complex variants of dark energy within standard gravity. It remains important to test the equivalence principle and General Relativity (GR) at cosmological scales.

The kind of MG models used to study gravity at large-scales predicts an extra fifth force which emerges by the presence of a new scalar field that modifies the structure formation at different scales. A general feature of the surviving models is that they often rely on screening mechanisms to suppress the fifth force in the solar system, centres of dark matter haloes, and in general, high density regions or small scales. This is true for both the $f(R)$ (Li & Barrow, 2007; Brax et al., 2008) and nDGP models (Dvali, Gabadadze & Porrati, 2000). The former features a chameleon screening and the latter the Vainshtein screening mechanism (Khoury & Weltman, 2004; Vainshtein, 1972). The inevitable alteration of structure formation in an environmental dependent manner, i.e. in the regime where the fifth force is suppressed, makes gravity behave as in GR and structure formation remains similar to that of the Λ CDM; in the places where the fifth force is unscreened, such as in low density regions in the $f(R)$ model, or outside the so-called Vainshtein radius in nDGP model, the additional fifth force changes structure formation in a complex way. This provides opportunities to test these models using statistics that are sensitive to the environment-dependent nature of structure formation. Thus, tests that involve weak lensing, large-scale structures as galaxy clusters or cosmic voids and measurements of redshift-space distortions could be useful to distinguish models of gravity. In this work, we explore using the marked correlation method to test gravity using the $f(R)$ model as an example, motivated by the methodology proposed in White (2016).

The marked correlation is a high order statistical method which contains information beyond the galaxy two point correlation function. It is useful for studying the connections between properties of galaxies, such as luminosity and environmental density, with the flexibility of the choice of the mark (e.g. Beisbart & Kerscher, 2000; Sheth & Tor-

men, 2004; Harker et al., 2006; Wechsler et al., 2006), that acts as weights when the clustering is computed. This kind of statistic has been applied to break degeneracies between the halo occupation and the σ_8 parameter in two different cosmological models with the same clustering (White & Padmanabhan, 2008). The same principle should be applicable to distinguish MG and Λ CDM (White, 2016), by computing the clustering of galaxies considering marks which contain information about the different environments, that depends on the strength of gravity or the fifth force. In this work, using galaxy catalogues from both $f(R)$ and Λ CDM simulations, that are tuned to have the same clustering, we explore different marked statistics to see if these models can be told apart.

The key question is what mark is the optimal to fulfill our task. We explore two quantities, local density and halo mass, which we believe should serve best for our purpose of capturing the difference due to the distinct environmental dependencies for structure formation in $f(R)$ and Λ CDM models. Previous works involving modified gravity tell us that cosmic voids grow larger in comparison to GR (Cautun et al., 2018) and dark matter halos are formed more efficiently when the fifth force is present (Cai, Padilla & Li, 2015). The outline of this work is the same as in Armijo et al. (2018) paper, which this thesis is based, as the following: In § 2 we describe $f(R)$ theory and our simulations. The results of the marked correlation function are shown in § 3. We draw conclusions and discuss our results in § 4.

Chapter 2

Theory and simulations

2.1 The $f(R)$ model of gravity

The MG model studied in this letter is $f(R)$ gravity (see De Felice & Tsujikawa, 2010, for a review) , which extends GR by including a function of the Ricci scalar R , $f(R)$, in the Einstein-Hilbert action:

$$S = \int d^4x \sqrt{-g} \left\{ \frac{1}{2\kappa^2} [R + f(R)] + \mathcal{L}_m \right\}, \quad (2.1)$$

where $\kappa^2 = 8\pi G$, G is Newton's constant, g is the determinant of the metric $g_{\mu\nu}$, and \mathcal{L}_m is the Lagrangian density for matter. By varying the action, we can obtain a modified version of the Einstein field equations

$$G_{\mu\nu} + f_R R_{\mu\nu} - g_{\mu\nu} \left[\frac{1}{2} f - \nabla^2 f_R \right] - \nabla_\mu \nabla_\nu f(R) = 8\pi G T_{\mu\nu}^m, \quad (2.2)$$

with $G_{\mu\nu}$ the Einstein tensor, ∇_μ the covariant derivative for the metric tensor, $f_R \equiv \frac{df}{dR}$ is the so-called scalaron and represents a new, scalar and dynamical degree of freedom, finally $T_{\mu\nu}^m$ is the energy-momentum tensor for matter. By taking the trace of Eq. (2.2), and under a quasi-static approximation, it is possible to obtain the equations of motion for f_R and the Newtonian potential Φ without dependence on time (Bose et al., 2015):

In this model, gravity between massive particles is governed by a modified Poisson equation:

$$\vec{\nabla}^2\Phi = \frac{16\pi G}{3}a^2[\rho_m - \bar{\rho}_m] + \frac{1}{6}a^2[R(f_R) - \bar{R}], \quad (2.3)$$

in which $\rho_m = \rho_m(\mathbf{x}, t)$ is the density of non-relativistic matter at scale factor a , an overbar means the cosmic mean of a quantity and $f_R \equiv df(R)/dR$ is an additional scalar degree of freedom (a scalar field) which is governed by an equation of motion (EoM):

$$\vec{\nabla}^2 f_R = -\frac{1}{3}[R(f_R) - \bar{R} + 8\pi G(\rho_m - \bar{\rho}_m)]. \quad (2.4)$$

which are dynamical equations for the scalaron field and a modified Poisson equation for Φ . Note that in both equations, the Ricci scalar is expressed as a function of f_R by the inverse of the $f_R(R)$ function. Eqs. (2.3) and (2.4) can be combined to obtain

$$\vec{\nabla}^2\Phi = 4\pi G a^2[\rho_m - \bar{\rho}_m] - \frac{1}{2}\vec{\nabla}^2 f_R, \quad (2.5)$$

which indicates that $-\frac{1}{2}f_R$ can be considered as the potential of a force, called the *fifth force*, that is mediated by the scalar field f_R .

The Chameleon Mechanism

An interesting feature of this model is the chameleon screening mechanism (Khoury & Weltman, 2004), which is activated in inside a deep Newtonian potential (e.g., the solar system) or with a uniform high matter density (e.g., the early Universe), the solution to Eq. (2.4) is dynamically driven to $|f_R| \rightarrow 0$ so that Eq. (2.5) reduces to the standard Poisson equation: in this regime GR is recovered, hence offering a way for the theory to pass stringent solar system tests of gravity.

In contrast, in shallow Newtonian potentials, the dynamics of Eq. (2.4) is such that $\delta R = R - \bar{R}$ is negligible, and Eq. (2.5) reduces to

$$\vec{\nabla}^2\Phi = \frac{16}{3}\pi G a^2[\rho_m - \bar{\rho}_m], \quad (2.6)$$

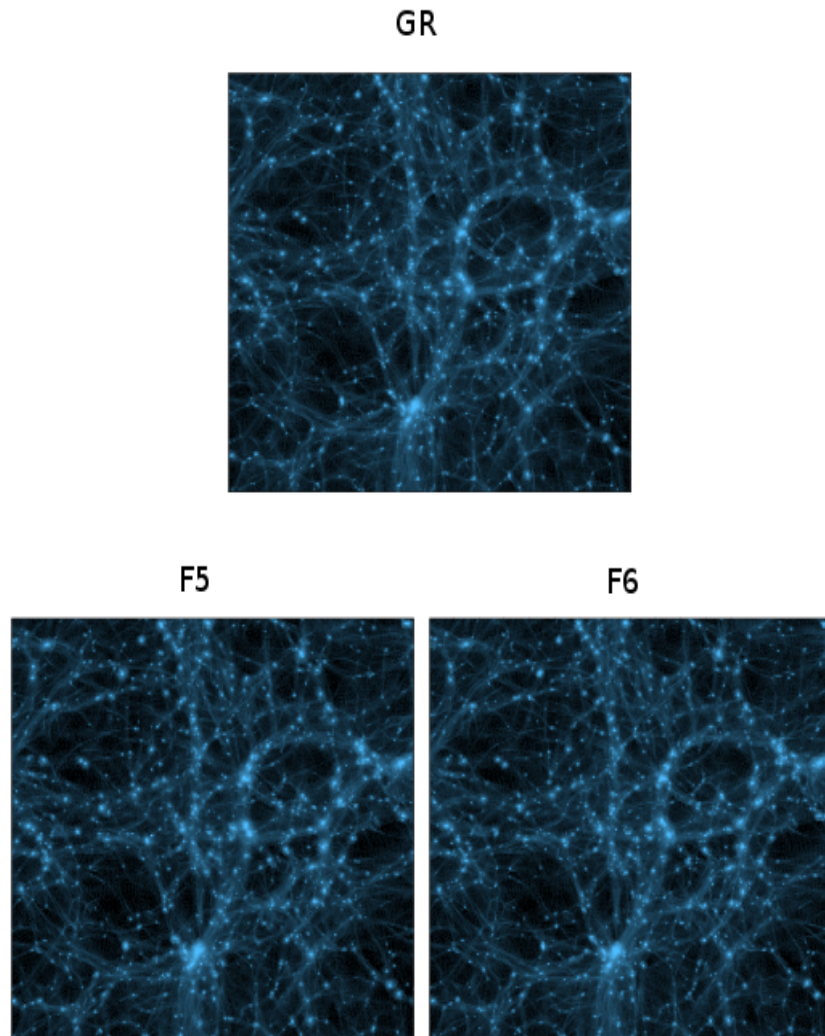


Figure 2.1: Dark matter particle simulations in a box with size of $64 \text{ Mpc}/h$, from Zhao, Li & Koyama (2011). A comparison between ΛCDM universe and modified gravity. Bottom panel are the two $f(R)$ models used in this work, with $|f_{R0}| = 10^5, 10^6$ respectively.

indicating a 1/3 enhancement of gravity with respect to GR, or a fifth force with 1/3 the strength of standard gravity at maximum, independent of the form of $f(R)$. This fifth force can enhance the growth of dark matter haloes (Cai, Padilla & Li, 2015), and make cosmic voids grow larger by evacuating more matter from void centres (Clampitt, Cai & Li, 2013). The fact that the fifth force is strong in low-density regions but suppressed in high-density regions implies that the difference from GR can be strengthened by up-weighting low density regions using marked statistics, thus offering a way to distinguish the model from Λ CDM. We shall show this is the next case, and for illustration, we adopt the form of $f(R)$ proposed in Hu & Sawicki (2007):

$$f(R) = -m^2 \frac{c_1(-R/m^2)^n}{c_2(-R/m^2)^n + 1}, \quad (2.7)$$

where $m^2 = \kappa^2 \bar{\rho}_0/3$, and $\bar{\rho}_0$ being the mean density of the Universe today.

For a realistic expansion history, $|R| \gg m^2$ for $z \geq 0$, so that

$$f(R) \approx -\frac{c_1}{c_2} m^2 + \frac{c_1}{c_2^2} m^2 \left(\frac{m^2}{R}\right)^n, \quad (2.8)$$

to a good approximation. If we set $c_1/c_2 = 6\Omega_\Lambda/\Omega_m$, where Ω_m is the density parameter for matter today and $\Omega_\Lambda = 1 - \Omega_m$, the model can accurately mimic a Λ CDM expansion history. Meanwhile,

$$f_R \approx -n \frac{c_1}{c_2^2} \left(\frac{m^2}{R}\right)^{n+1}, \quad (2.9)$$

can be inverted to find $R(f_R)$ which is used in Eqs. (2.3, 2.4). Thus the model has two free parameters, n and c_1/c_2^2 , which can be related to the value of f_{R0} today by using Eq. (2.9):

$$\frac{c_1}{c_2^2} = -\frac{1}{n} \left[3 \left(1 + 4 \frac{\Omega_\Lambda}{\Omega_m} \right) \right]^{n+1} f_{R0}. \quad (2.10)$$

A smaller $|f_{R0}|$ means weaker deviation from GR. The current cosmological constraint on these parameters is and $|f_{R0}| \lesssim 10^{-5}$ (e.g. Cataneo, M. et al., 2015; Liu et al., 2016); we fix $n = 1$ in this work as is suggested in the literature given the current cosmological constrains.

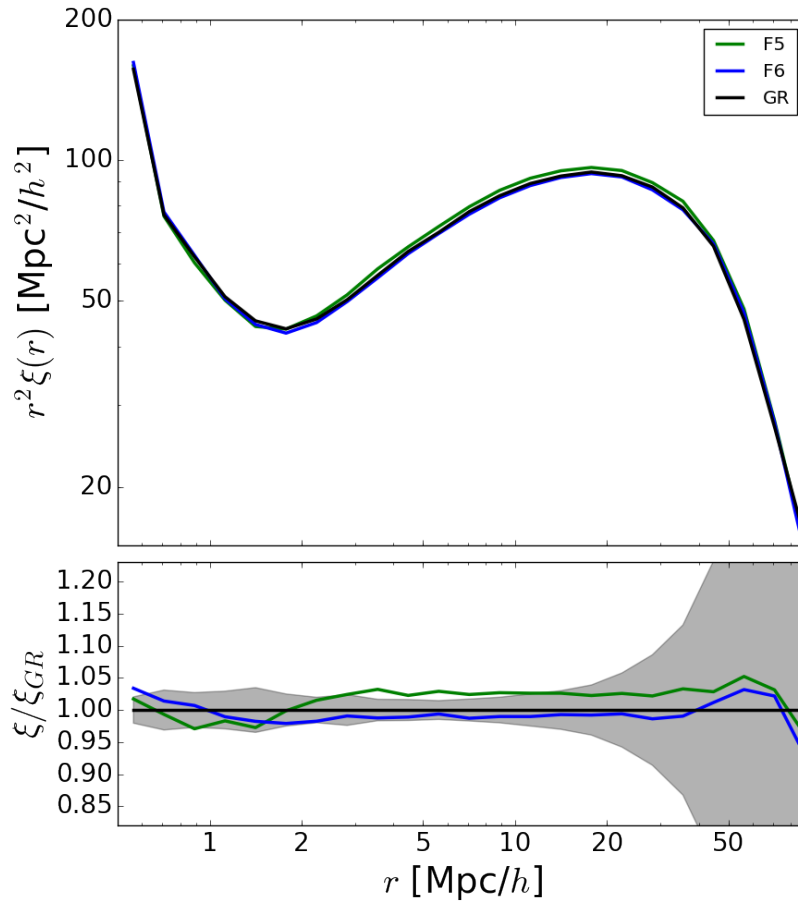


Figure 2.2: The two-point correlation function ξ of the different model in the simulations. The shaded region indicates the 1σ confidence of GR model. As reported in Cautun et al. (2018) the clustering deviations between MG and GR models are below the 5%.

2.2 Simulations and mock galaxy catalogues

The simulations we employed here were run using the ECOSMOG code (Li et al., 2011), with 1024^3 dark matter particles with mass $m_p \approx 7.8 \times 10^{10} h^{-1} M_\odot$ in a box with size $L = 1024 h^{-1} \text{Mpc}$. We have 5 independent realizations for error analysis. Both $f(R)$ and GR models adopt the same ΛCDM background cosmology with parameters from the WMAP mission 9-yr results (Hinshaw et al., 2013), hence they essentially have the same expansion history and start from identical initial conditions, as is showed in Fig. 2.1. Two $f(R)$ models with different amplitude $|f_{R0}|$ are used in this work and are referred to as F5 and F6 (with amplitude values of $|f_{R0}| = 10^{-5}, 10^{-6}$ respectively). More details can be found in Cautun et al. (2018). Dark matter haloes were identified by using the ROCKSTAR code (Behroozi et al., 2013) with mass definition M_{200c} , where the subscript $200c$ refers to 200 times of the critical density of the Universe. There are no galaxies produced in the simulation until this stage.

We populated haloes with galaxies using a 5-parameter halo occupation distribution (HOD) recipe (Zheng et al., 2004). The procedure is as follows (see more details in Cautun et al., 2018; Li et al., 2017): For GR, we adopted the parameters from Manera et al. (2013), which were calibrated to match the SDSS CMASS clustering. We adjusted the HOD parameters for the $f(R)$ models to best match the galaxy numbers and two-point correlation functions in GR, this allow us to constrain MG and GR models in terms of galaxy clustering and number density as is observed in the Universe. The flexibility of the HOD model allows us to adjust the shape and magnitude of the galaxy two point correlation function by sampling haloes of different masses, as shown by the histogram for the mass of haloes hosting HOD galaxies by different models in Fig. 3.1. This process brought the agreement for the correlation functions ξ among different models to $\leq 2 \sim 3\%$ on scales of between $2 - 80 h^{-1} \text{Mpc}$ as is showed in Fig. 2.2. This was calculated as the rms difference between the GR and $f(R)$ correlation functions in all

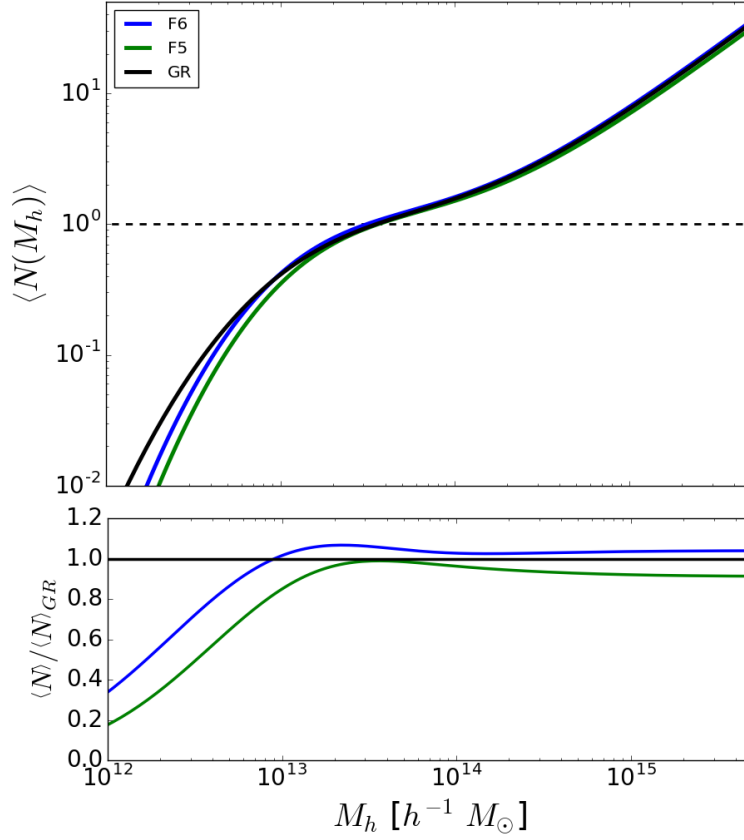


Figure 2.3: The mean number of galaxies, $\langle N \rangle$, as a function of halo mass, M for F5, F6 and GR models. The secondary panel shows the ratio of the $f(R)$ models HOD to the GR one. This parameters are used to match the clustering and number density of galaxies as is mentioned on Cautun et al. (2018)

galaxy separation bins (bottom panel of 2.2), and we also included in the calculation the difference in the galaxy number densities in these models. This agreement is the best we can get with the 5-parameter HOD method using a simplex algorithm to find the best fit value of the HOD parameters. The plot of the number of the mean number of haloes as function of its mass is showed in 2.3.

Note the match for the galaxy correlation functions is in real space with no redshift space distortions. This is equivalent to matching the projected two-point correlation functions, as explained in Cautun et al. (2018). It is also worth noting that the correlation functions agree with each other within the errors estimated from a volume of $\sim 1(h^{-1}\text{Gpc})^3$ of our simulations, specifically for the catalogues used on this work, which correspond to $z = 0.5$, which is the redshift where the CMASS catalogue is centered. Considering the previous aspects, these simulations are consistent with some relevant observables in cosmology, such as the cosmological parameters from WMAP, and the clustering of SDSS CMASS galaxies, but also including distinct models of gravity.

Chapter 3

The Marked Correlation Function

3.1 Marked pairs computation

The marked correlation function is in essence a weighted version of the two point correlation function, where the weight is the mark m (e.g. Sheth et al., 2005; White, 2016)

$$\mathcal{M}(r) = \frac{1}{n(r)\bar{m}^2} \sum_{ij} m_i m_j, \quad (3.1)$$

where $n(r)$ is the number of pairs at separation r in real space, \bar{m} is the mean mark value computed for all the galaxies in the simulation and $m_i m_j$ is the product of the marks for the ij -galaxy pair. Note that on large scales the average over all pairs tends toward \bar{m}^2 , so \mathcal{M} becomes close to unity.

To compute the marked pairs at different scales, a two-point statistic code has been developed and can be found in the following URL: <https://github.com/bartok10/MarkedCF>. This C routines use the Davis & Peebles estimator (Davis & Peebles, 1983), to compute both the two-point correlation function and its marked version, in 3D co-moving coordinates with periodic boundary conditions. The code can be used in large galaxy simulations ($\sim 1h^{-1}\text{Gpc}$) and is in agreement with current algorithms in literature. (e.g the CUTE code in Alonso, 2012, being the most popular one).

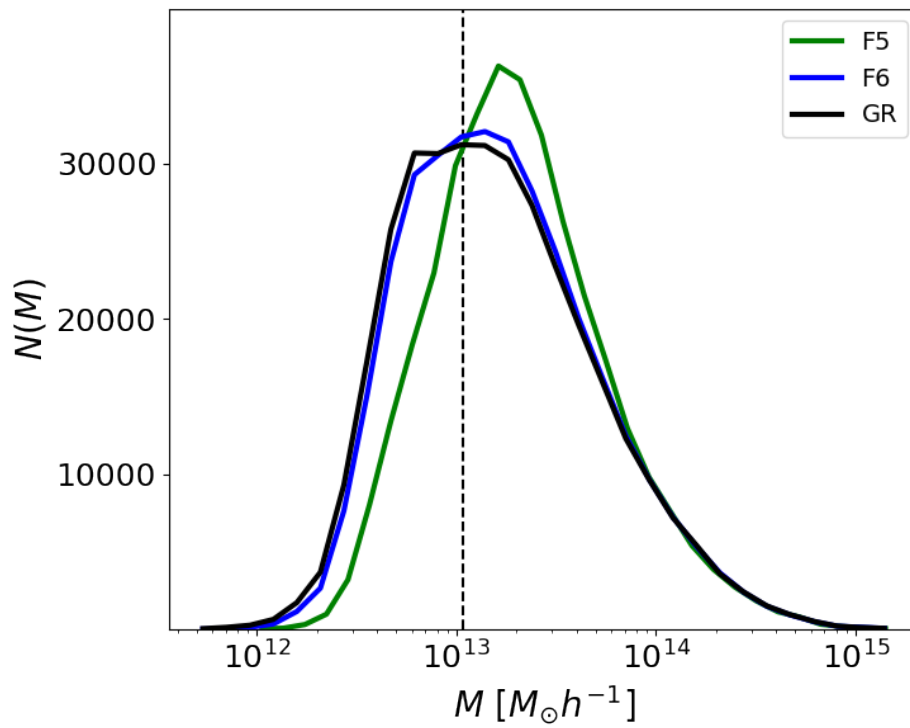


Figure 3.1: The distribution of the host halo mass M sampled by the HOD galaxies for different models as labelled in the legend. The dashed line indicates mean value for GR.

We use the local galaxy number density and the halo mass to define the marks in order to best capture the environmental dependence of structure formation induced by the chameleon screening mechanism in $f(R)$ models.

3.2 A mark based on local density

It is well known that for the $f(R)$ model the 5th force is unscreened in low density regions such as voids (e.g., Hui et al., 2009; Clampitt, Cai & Li, 2013). The consequence is that voids expand faster and become emptier than in GR. The change of large-scale structure in low density regions may not be detectable in the galaxy two point correlation function, which results from the global average of all galaxy pairs. This is because tracers in low density regions have lower amplitudes of clustering by definition, and so their contribution to the total correlation function is minor. As a result, the effect of the chameleon screening may have been hidden under the globally averaged two point correlation function. To amplify the effect due to screening, it is therefore useful to use the local density as a mark, in particular, to up-weight the low density regions.

To do this, we use Voronoi tessellations from the ZOBOV code (Neyrinck, 2008) to estimate the density around each galaxy. The density of a galaxy ρ_i is inversely proportional to the volume of each Voronoi cell V_i . Fig. 3.2 shows the distribution of galaxy local densities estimated in this way. It is clear that while the distributions remain similar to each other for different gravity models for densities close to the mean, $f(R)$ models tend to have more galaxies with low densities, i.e. the most isolated galaxies in $f(R)$ models are even more isolated than in GR. In particular, the number of galaxies with $\rho_i < 0.2$ could be a factor of 2-3 higher for F5 than for GR. For F6, the difference from GR is milder but the trend is the same. This confirms the expectation that the abundance of low density regions is larger in $f(R)$ models even when the galaxy two

point correlation functions are the same as in GR. It suggests that having a mark to up-weight the low density regions to enhance this effect may be useful to distinguish $f(R)$ models from GR.

We first try the mark defined by $m_i = \rho_i^p$ where the power index p is chosen to be negative to up-weight low density regions. An example for $p = -0.5$ is shown in Fig. 3.3 (solid line). For F5, the marked correlation function is above the GR version at the $\sim 2\sigma$ level at small scales, consistent with the fact that the probability of low density galaxies are higher in this model. For F6, however, it is consistent with GR within the errors, due to the relatively small difference from GR in the distribution function of densities.

These results change with the value of p . When p is more negative, e.g. $p < -1$, more weights will be assigned to the low density regions. The relative difference between models becomes larger but the noise also increases, because the number of low density galaxies is small. On the other hand, when p is positive, e.g. $p > 0.5$, more weights will be assigned to high density regions, which are also rare. In this case, the marked correlations become noisy and indistinguishable from one model to another within the errors. For comparison, an example for $p = 0.5$ is also shown in dashed curves in Fig. 3.3. The light-shaded region in the bottom shows the errors on the mean corresponding to a volume of $\sim 1(h^{-1}\text{Gpc})^3$. These errors are estimated using the jackknife method with all the 5 simulation boxes. The errors are much larger than the case of $p = -0.5$, indicating that the large overdense regions are rarer or higher in their amplitudes than the underdense ones, and so the Poisson noise becomes much larger when up-weighting high densities. Both the F6 and F5 curves are broadly consistent with GR within the errors. This confirms the fact that the distribution of galaxies differs more in underdense regions than in overdense regions, and the former carries more information about MG. We have also repeated the same analysis with galaxies in redshift space and find that the marked correlation functions become noisier, but results remains qualitatively similar to those in real space.

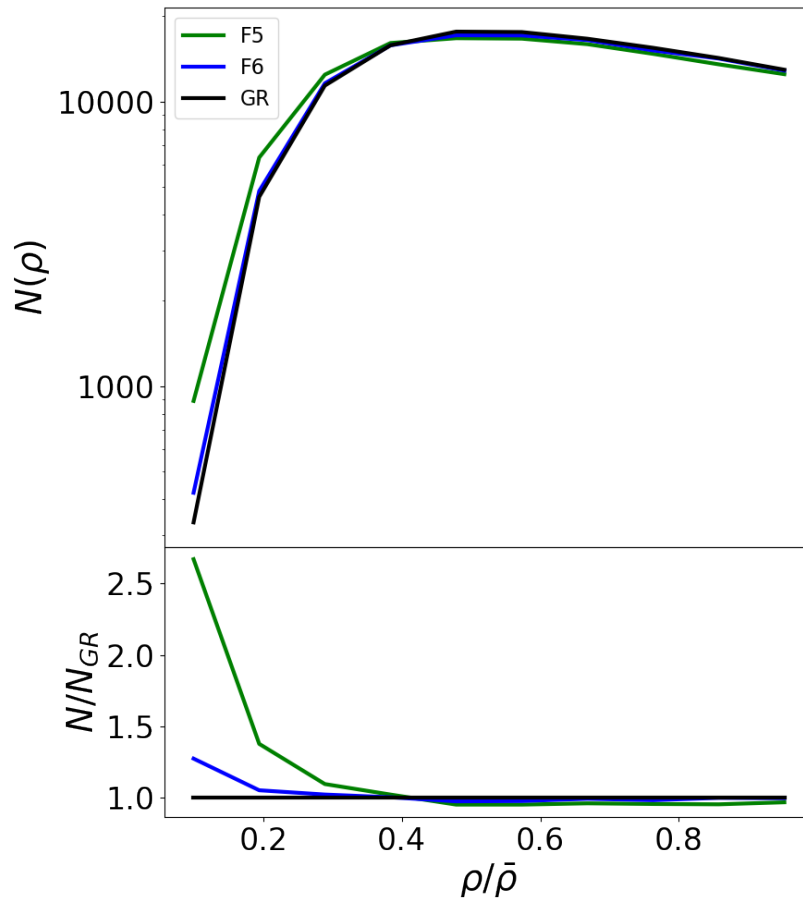


Figure 3.2: Distribution of galaxy local densities estimated using a Voronoi tessellation method. Only the range of below the mean density is shown for better illustration.

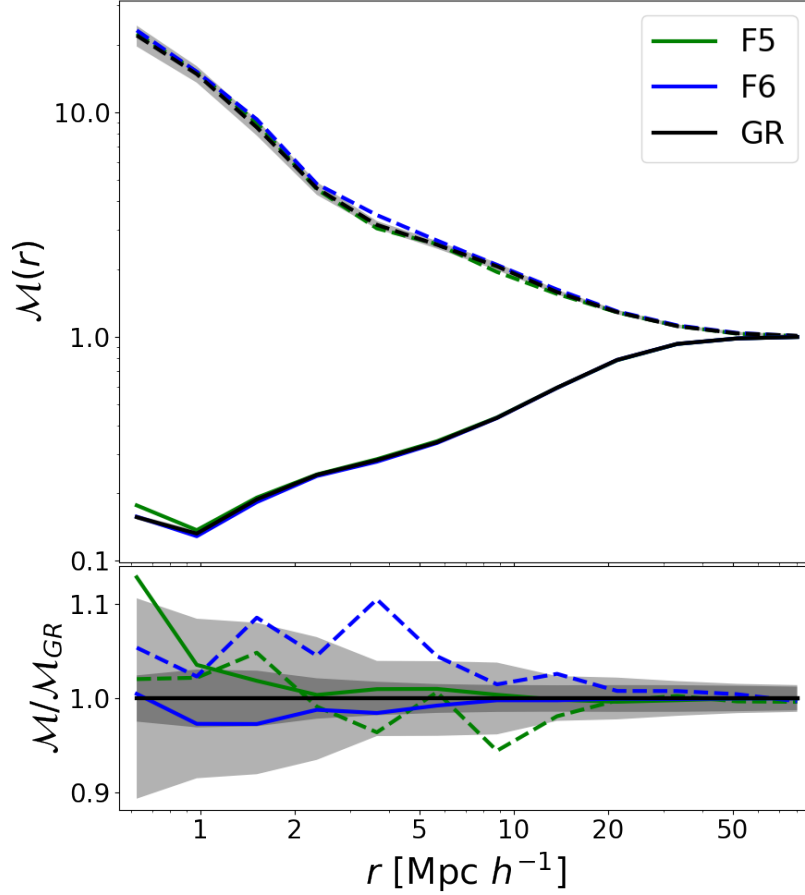


Figure 3.3: The marked correlation function $\mathcal{M}(r)$ using the local density ρ as the mark. This plot shows the examples for $\mathcal{M} = \rho^p$, with $p = \pm 0.5$ in solid (-0.5) and dashed lines (0.5). The lower panel shows the ratios of marked correlation functions between $f(R)$ and GR. The shaded regions correspond to the errors on the mean corresponding to a volume of $\sim 1(h^{-1}\text{Gpc})^3$ estimated using the Jackknife method. The dark and light shaded regions are for the case of $p = -0.5$ and $p = 0.5$ respectively.

3.3 A mark based on halo mass

Due to the fifth force, the halo mass functions in $f(R)$ gravity and GR are different (e.g., Cataneo et al., 2016). The halo occupancies of galaxies, therefore, have to compensate for this in order to have the same galaxy clustering and number density. This inevitably induces differences in the underlying halo populations being occupied by galaxies, as shown in Fig. 3.1.

Another way to see this is that there are differences in the relations between the galaxy and halo populations in these models. Matching the galaxy density and clustering will result in haloes being populated differently in these models. On the other hand, one can in principle change the HOD parameters such that the halo populations being sampled are the same for different models, but then the galaxy clustering will be different. This difference in the intrinsic relation between haloes and galaxies offers an opportunity to distinguish these two types of models by having a joint constraint from galaxy clustering and their underlying halo population. By using halo mass as the mark in the marked correlation function we can achieve this goal.

To do that, we simply set $m_i = M_i^p$, where M_i is the mass of the host halo, and the index p is a free parameter of our choice. We explore a wide range of p and find that F5 can be well distinguished from GR with $0.001 < |p| < 0.1$. An example for $p = \pm 0.1$ is shown on the left-hand panel in Fig. 3.4. The marked correlation function for the F5 model deviates from the 1σ region of the GR version at scales as large as $20h^{-1}\text{Mpc}$, which is well beyond the 1-halo term region. The results remain similar in the above range of p : the amplitude of the marked correlation function decreases with $|p|$, but the errorbars also decrease by approximately the same factor. Therefore, the significance for the deviation from GR is rather independent of p . When $|p|$ is relatively large, i.e. $|p| > 0.1$, the measurement becomes noisy because the tail of the mass distribution is up-weighted regardless of the sign of p . This is because the distributions of halo mass

sampled by the HOD peak at approximately $10^{13}h^{-1}M_{\odot}$ and drops rapidly towards both the low and high mass ends (Fig. 3.1) This enhances the Poisson noise and makes F5 indistinguishable from GR at $|p| > 0.1$. In the limit when $|p| \approx 0$, the mark becomes flat and the correlation functions are equal to unity for all models, and they become indistinguishable from each other. For all the cases we have explored, F6 is always consistent with GR within the errors.

The above experiment suggests a powerful way to constrain the $f(R)$ model, but it requires information about the host halo mass for each galaxy, which is not easily accessible from observation. Even if it is, there will be uncertainties on the halo mass. We therefore make two tests. First, we explore the case where uncertainties for the halo masses are added, i.e. $\log_{10} \tilde{M}_i = \log_{10} M_i + \Delta M$, where $\Delta M = \sigma$ is drawn from a Gaussian distribution with σ chosen to be 0.1, 0.2, 0.3. We then measure the marked correlation functions using these noisy marks. We find that the results remain qualitatively similar to the case with no noise in terms of the significance for the difference between F5 and GR. As the noise level increases, the errorbars increase as expected. At $\sigma = 0.3$, F5 is almost indistinguishable from GR. We show in the panels A & B of Fig. 3.4 the example for $\sigma = 0.1$ & 0.2.

Second, we explore the situation where haloes are binned into 8 mass bins, ranging from 10^{12} to $10^{15}h^{-1}M_{\odot}$, with a bin-width of half a decade. Note that errors for the halo masses have been added before they are grouped into mass bins. The mean mass of host haloes can be estimated either with galaxy-galaxy lensing (e.g. Han et al., 2015; Viola et al., 2015) or a dynamical method for stacked samples of galaxy groups (e.g. Kaiser, 1986; Carlberg et al., 1997; Evrard et al., 2008; Mamon et al., 2013). We then assign galaxies within each mass bin the same mark based on the median mass of the bin, and measure the marked correlation functions. We find that the results remain similar in terms of the differences between the two models, as shown in panels C & D of Fig. 3.4. Based on these tests, we conclude that using the halo mass as the mark is a stable and

powerful method for distinguishing $f(R)$ and GR models.

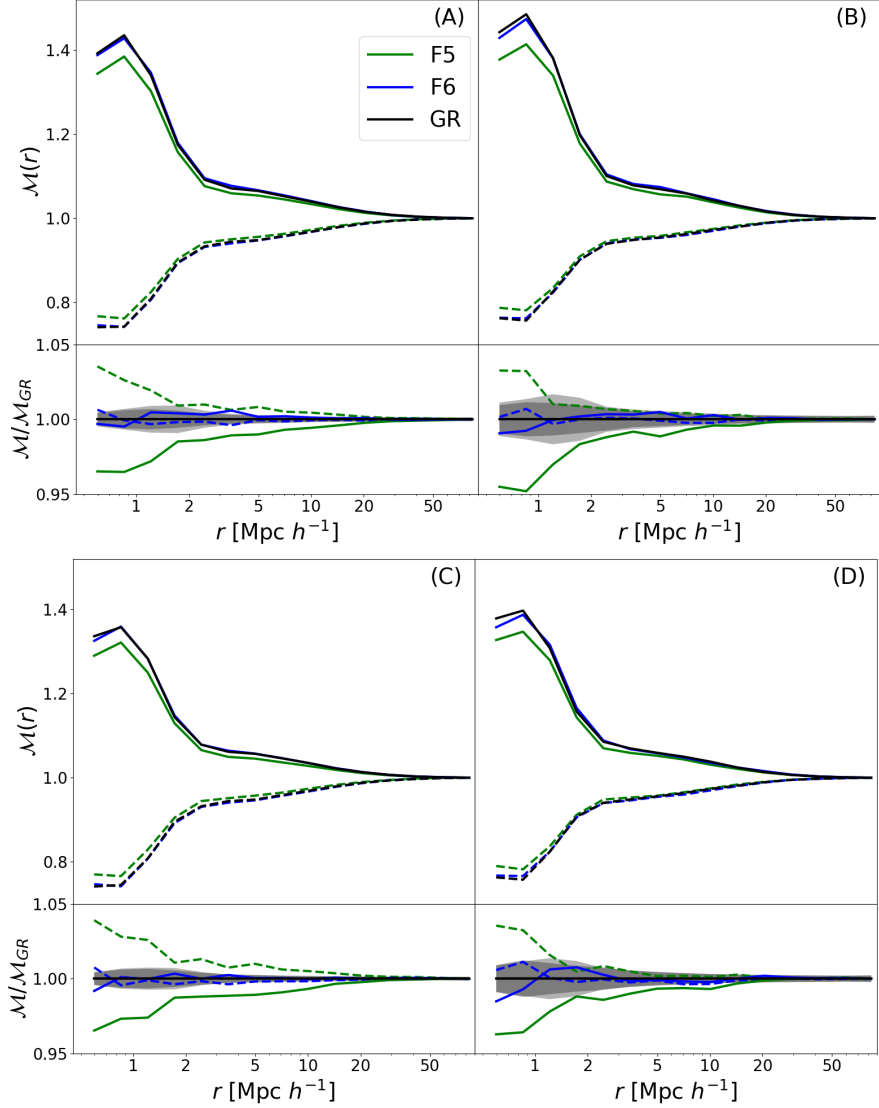


Figure 3.4: Similar to Fig. 3.3 but showing the marked correlation function using the host halo mass of galaxies M as the mark, $m = M^p$. The solid and dashed curves shows the case for $p = 0.1$ and $p = -0.1$ respectively. The dark and light shaded regions show the 1σ errors for these two cases. The panels show the different cases: using the host halo mass as mark adding 0.1 dex uncertainty to the masses (A), adding 0.2 dex uncertainty (B), using only 8 mass bins to generate the marks and 0.1 dex uncertainty (C) and adding 0.2 dex uncertainty (D).

Chapter 4

Conclusions and Discussion

4.1 Discussion

When the mark is defined, an exponent p is included as a free parameter to control the amplitude of the marked correlation function. In principle, the choice on the value of p would affect statistically on how different are the marked correlation functions between the models. We use the reduced χ_ν^2 statistic to capture the differences between MG and GR models for different values of p . This requires the computation of the covariance matrices for both, the standard correlation function and its marked version. The analysis is made by assuming GR as a fiducial model of Λ CDM cosmology, which is compared with F5 and F6 models representing the $f(R)$ cosmology. The reduced χ_ν^2 is obtained from

$$\chi_\nu^2 = \frac{1}{\nu} \sum_{ij}^n \Delta^i C^{ij-1} \Delta^j, \quad (4.1)$$

where ν is the number of degree of freedom, $\Delta^i = \xi_{GR}^i - \xi_{MG}^i$ or $\Delta^i = \mathcal{M}_{GR}^i - \mathcal{M}_{MG}^i$, and the covariance matrix C^{ij-1} for the unmarked or marked correlation function respectively.

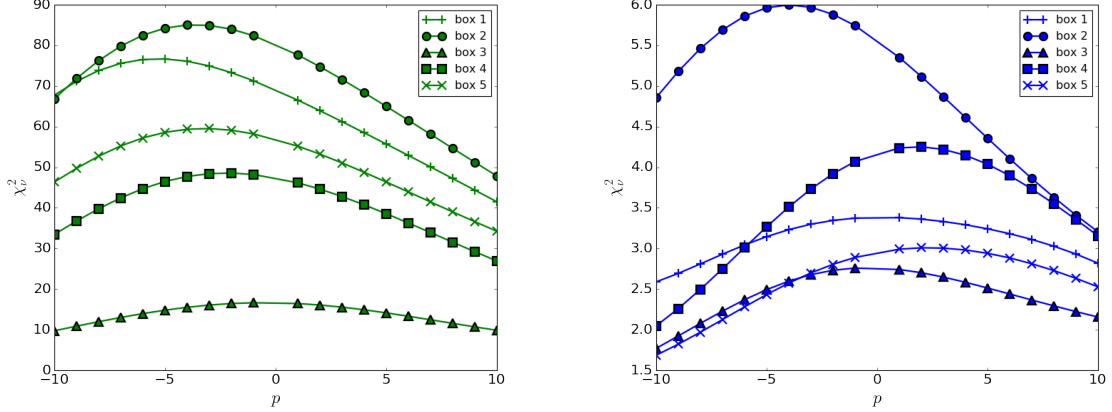


Figure 4.1: Different χ^2_ν as function of the free parameter p for the mass-marked correlation function in F5 (*left*) and F6 (*right*). The 5 boxes show a wide range of possible χ^2_ν values in a range of $p = [-10, 10]$.

In this analysis, the χ^2_ν value is used as a goodness of fit to determine how similar is the two-point correlation function in the different cosmologies, expecting a value of $\chi^2_\nu \sim 1$, for both F5 and F6 models. In the other hand, for the marked correlation function a value of $\chi^2_\nu > 1$ is expected, this tell us how much different the models are at level of σ . For our models of marks, we set the free parameter p to up-weight different regimes or scales that depends on the environment. As we mention in the Section 3.2 and Section 3.3 the parameter p handle both the amplitude of the marked correlation function and the size of the errors, which means there is a dependence between the χ^2_ν value and p . In Fig. 4.1 the χ^2_ν value for the different values of p are showed. Although, there is not a preferred value of p for the different boxes or the two $f(R)$ models, there is a tendency of maximize the χ^2_ν between $p = -2, -1, 1, 2$. Just for convenience we set $p = -1, 1$ to compute the mass-marked correlation function. In the case of the density-marked correlation function, the situation is similar but with smaller values of χ^2_ν given the higher noise as was explained in Sec. 3.2.

4.2 Conclusions

We have explored how to use the marked correlation function to distinguish $f(R)$ models from the Λ CDM universe using N-body simulations. Our study uses different halo occupancies to reproduce the observed projected galaxy two point correlation functions in different models of gravity. We explore two different marks related respectively to the local galaxy number density and host halo mass, and test their ability to distinguish the models. We find that up-weighting low density regions helps to unveil differences hidden in the correlation function, but only at relatively low significance and on small scales. The latter are actually in the regime of the one-halo term, which can be difficult to interpret in redshift space. Nevertheless, this is qualitatively consistent with the expectation that low-density regions are influenced more strongly by the fifth force in $f(R)$ models.

The method of up-weighting low density regions is in the same spirit of testing gravity using voids (Clampitt, Cai & Li, 2013; Cai, Padilla & Li, 2015), clipping off peaks (Lombriser et al., 2015), or doing a log transformation on the density (Llinares & McCullagh, 2017). It also achieves similar goals to the position-dependent power spectrum method in capturing information about three-point statistics (Chiang et al., 2014). Our study differs from the recent work of Valogiannis & Bean (2017) (VB) where the marked correlation function method was applied to simulations of $f(R)$ and Symmetron models in the following: VB apply the marked statistic to the matter density fields, while we use mock galaxy catalogues, calibrated to have the same clustering and number densities among different models. This sets different requirements for implementing these techniques in observations.

We find much stronger deviations between the different models when using halo mass to define the mark. The difference is found out to larger scales ($\sim 20h^{-1}\text{Mpc}$) with higher significance. Our forecast is based on a simulation volume of the same order

as that of the SDSS CMASS galaxy sample. The constraining power of our approach for the model comes from the quasi-linear and non-linear regimes. Our method offers compatible constraints for the $f(R)$ model compared to other independent approaches such as matter bispectrum (Gil-Marín et al., 2011), stacked phase-space distribution (Lam et al., 2012) and galaxy infall kinematics (Zu et al., 2014) over a similar range of scales. It promises better constraints than that from the large-scale linear regime, such as galaxy power spectrum (Dossett et al., 2014), redshift-space distortion (Yamamoto et al., 2010) and the Integrated Sachs-Wolfe effect (Song et al., 2007; Lombriser et al., 2012) (see also Lombriser, 2014, and references therein).

Similar conclusions were found by an independent study (Hernandez-Aguayo et al., 2018) following a similar approach. When using halo mass as the mark we find the result to be stable for a wide range of power indices. The significance remains similar when errors are introduced into the halo mass, or when haloes are grouped into mass bins mimicking stacking to obtain masses via weak lensing, as the method does require additional information about the host halo mass of galaxies. The host halo mass can in principle be measured using a dynamical method or weak gravitational lensing. The latter requires overlapping of a lensing survey and a spectroscopic redshift survey over the same sky. Existing surveys such as GAMA plus KiDS are essentially ready for performing this measurement (Driver et al., 2011; Hildebrandt et al., 2017). In principle, the total mass of haloes will be affected by baryonic effects, which may change the mass of haloes by a few percent and up to 20 percent in the mass range of haloes of our interest (e.g. Schaller et al., 2015). The impact of this on the marked correlation function needs to be investigated in a self-consistent manner for different models of gravity, which is beyond the scope of this work.

4.3 Proposed application to data

The next step after this study is to think about how the marked correlation function can be applied to observational data. One thing to consider, which should be the most important aspect to determine, is what sample of galaxies can be used on purposed to complete such a test. Additionally, a proper mark m need be chosen to include all the environmental information that can be used to rule out MG models. If we think about the marks used in this work, both the local density ρ and the host halo mass M , can be applied only in large surveys of galaxies, focused in large-scale structures and baryon acoustic oscillation measurements, as the current extended Baryon Oscillation Spectroscopic Survey (eBOSS) (Dawson et al., 2016) and future surveys as LSST (LSST Dark Energy Science Collaboration, 2012) and DESI (Levi et al., 2013). In the case of using the local density to compute the marked clustering the difficulties come by obtain systematics errors given projection effects or by redshift space distortions, that would add noise to the marked correlation function, making it not statistically significant to rule out or constrain $f(R)$ models. The other possibility is to use the mass of host halos to mark the clustering of galaxies in groups. Precise measurements of halo masses are required, and this can be accomplished by taking weak lensing or dynamics methods or another independent way to measure the mass with precision. In this context, galaxy clusters represent good candidates as their mass measurements are robust and can be modeled as high mass halos. In the 14th data release (DR14) of SDSS-IV the SPIDERS program (Clerc et al., 2016) offers the potential sample of candidates to apply the marked correlation function. The SPIDERS clusters present masses estimations given x-ray luminosities, which are confirmed by velocity dispersion measurements of the galaxy cluster members, currently the sample is about 1200 galaxy clusters. If we combine this cluster sample with eBOSS spectroscopic galaxies, a marked-cross-correlation function can be computed using the local density estimation as mark of the galaxies and the

mass of cluster as mark for the galaxy cluster centres. This can be easily tested in our simulations by taking the most massive halos in MG and GR models ($M > 10^{14}M_{\odot}$) and considering the same clustering in terms of the unmarked cross correlation function version. The marked-cross-correlation function for the galaxies in the simulation using halo masses and local density as marks is showed in Fig. 4.2. Although small deviations can be found between the models, the errors are small, which tell us that the marked-cross correlation function captures the same kind of information as the version showed in Fig. 3.4. Such a test can be used to constrain modified gravity models precisely, as galaxy clusters are extremely good probes to test both gravity and cosmic acceleration.

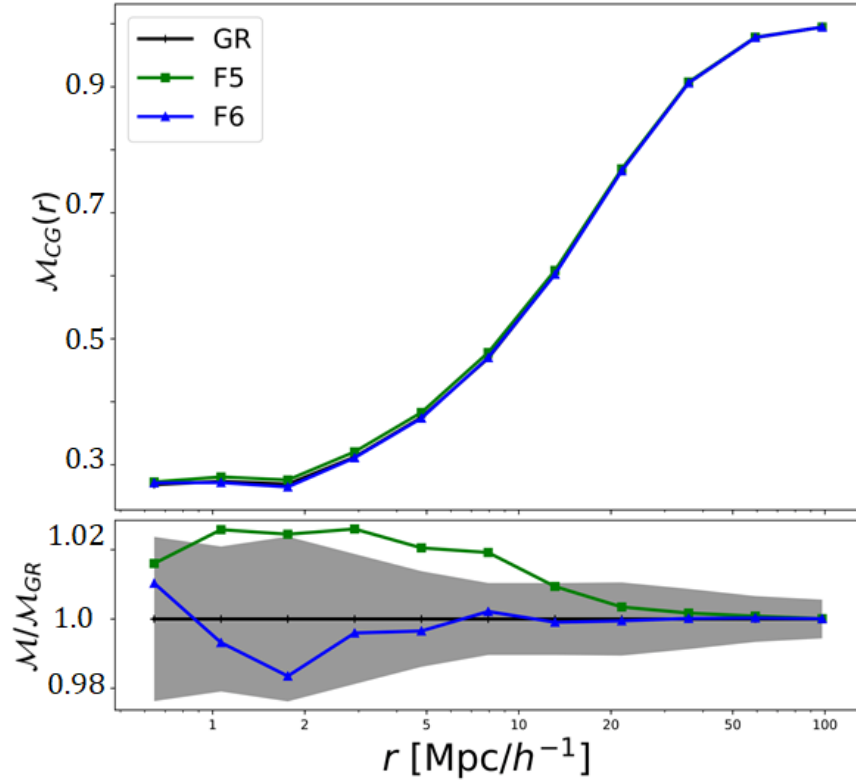


Figure 4.2: The marked-cross-correlation function between GC centers and galaxies for different models. A combination of marks is explored in this case, using $m_{GC} = M^p$ and $m_g = \rho^p$. The shaded region is the GR errorbars estimations showing the 1σ confidence estimation.

Bibliography

Lombriser, L. and Taylor, A. JCAP. 3,31 (2016).

Baker, T. et al., ArXiv e-prints, eprint: 1710.06394, 2017.

Sakstein, J. and Jain, B. ArXiv e-prints, eprint: 1710.06394, 2017.

Ezquiaga, M. and Zumalacarregui, M. ArXiv e-prints, eprint: 1710.05901, 2017.

Creminelli, P. and Vernizzi, F. ArXiv e-prints, eprint: 1710.05877, 2017.

De Felice, A. and Tsujikawa, S. Living Rev. in Relativity, 13, 2010.

Dvali, G. Gabadadze, G. and Porrati, M. Phys. Letters B (2000), 484, 112-118.

Li, B. and Barrow, John D., Phys. Reviews (2007), D75, 08410.

Brax, P. et al. Phys. Reviews (2008), D78, 104021.

Khourym J. and Weltman, A., Phy. Rev. D (2004), 69, 4, 26-44.

Vainshtein, A.I., Physics Letter B (1972), 39, 3, 393-394.

White, M. JCAP (2016), 1611, 11, p-57.

Beisbart, C. and Kerscher, M., APJ (2000), 545, 6-25.

Sheth, R.K., Tormen, G., MNRAS (2004), 350, 1385-1390.

- Harker, G. et al., MNRAS (2006), 367, 1039-1049.
- Wechsler, R.H. et al. APJ (2006), 652, 71-84.
- White, M. and Padmanabhan, N. MNRAS (2008), 395, 2381-2384.
- Abbott, B. P. et al. ApJ Letters. (2017), 848, 2.
- Cautun, M. et al. MNRAS (2018), 476, 3, 3195-3217.
- Cai, Y.-C., Padilla, N. and Li, B. MNRAS (2015), 451, 1036-1055.
- Armijo, J. et al., MNRAS (2018) DOI:10.1093/mnras/sty1335.
- Clampitt, J. Cai, Y.-C. Li, B., MNRAS (2013), 431, 749-766.
- Hu, W. and Sawicki, I. Phys. Rev. D (2007), 73,6.
- Cataneo, M. et al. JCAP (2016), 1612,12.
- Liu, X. et al. Phys. Rev. Lett. (2016), 117,5.
- Li, B. et al. JCAP (2012), 1201,1475.
- Hinshaw, G. et al. ApJ (2013), 208.
- Behroozi, P. et al. ApJ (2013), 762.
- Zheng, Z. et al., ApJ (2004), 633, 791-809.
- Li, B. et al. ArXiv e-prints, eprint:1710.07291.
- Manera, M. et al. MNRAS (2013), 428, 2, 1036-1054.
- Sheth, R. et al. ArXiv e-prints, eprint:0511773.
- Hui, L. et al. Phys. Rev. D (2009), 80, 10.

- Cataneo, M. et al. JCAP (2016), 12, 24.
- Neyrinck, M. MNRAS (2008), 386, 2101-2109.
- Han, J. et al. MNRAS (2015), 446, 1356,1379
- Viola, M. MNRAS (2015), 452, 3529-3550.
- Kaiser, N. MNRAS (1986), 222, 323-345.
- Carlber, R. ApJ (1997), 478, 462-475.
- Evrard, A. et al. Apj (2008), 672, 122-137.
- Mamon, A. MNRAS (2013), 429, 3079-3098.
- Lombriser, L. et al. Phy. Rev. Letters (2015), 114, 25.
- Llinares, C. and McCullagh, N. MNRAS (2017), 472, L80-L84.
- Chiang, C. et al. JCAP (2014), 5, 48.
- Valogiannis, G. and Bean, R. Phys. Rev. D (2017), 97,2.
- Gil-Marin, H. et al. JCAP (2011), 11, 19.
- Zu, Y. et al. MNRAS (2014), 445, 1885-1897.
- Dossett, J. et al. JCAP (2014), 3, 46.
- Song, Y. et al. Phy. Rev. D. (2007), 76, 6.
- Lombriser, L. et al. Phy. Rev. D. (2012), 85, 12.
- Lombriser, L. Annalen der Physik (2014), 526, 259-282.
- Lam, T. et al. Phy. Rev. Lett. (2012),109, 5

- Yamamoto, K. *Phy. Rev. D.* (2010), 81, 10.
- Hernández-Aguayo, C. et al. *ArXiv e-prints* (2018), eprint: arXiv:1801.08880.
- Driver, S. et al. *MNRAS* (2011), 413, 971-995.
- Hildebrandt, H. et al. *MNRAS* (2017), 465, 1454-1498.
- Schaller, M. et al. *MNRAS* (2015), 451, 1247-1267.
- Bose, S. et al. *JCAP* (2015),2,34.
- Dawson, K. and the eBOSS collaboration. *AJ* (2016) 151,44.
- LSST Dark Energy Science Collaboration, *ArXiv e-prints*, 1211.0310.
- Levi, M. and DESI collaboration, *ArXiv e-prints*, 1308.0847.
- Clerc, N. et al. *MNRAS* (2016), 463, 4, 4490-4515
- Davis, M., and Peebles, P. J. E. (1983), *ApJ*, 267, 465
- Alonso, D. *ArXiv e-prints* 2012, 1210.1833.
- Zhao, G.-B., Li, B., Koyama, K. *Phys. Rev. D* 83, 2011